APS physics

CHORUS

This is the accepted manuscript made available via CHORUS. The article has been published as:

Measurement of stray electric fields in a capacitive inertial sensor using contactless test-mass charge modulation

S. M. Apple, S. Parry Kenyon, S. Barke, M. R. Clark, A. Y. Davila, B. C. Letson, G. Mueller, T. J. Olatunde, J. Sanjuan, O. E. Sauter, J. Siu, T. J. Sumner, P. J. Wass, and J. W. Conklin

Phys. Rev. D **106**, L101101 — Published 28 November 2022

DOI: 10.1103/PhysRevD.106.L101101

Measurement of Stray Electric Fields in a Capacitive Inertial Sensor using Contactless Test-Mass Charge Modulation

S. M. Apple[1], S. Parry Kenyon[1], S. Barke[1], M. R. Clark[1], A. Y. Davila[1], B. C. Letson[1], G. Mueller[1], T. J. Olatunde[1], J. Sanjuan[1], O. E. Sauter[1], J. Siu[1], T. J. Sumner[1,2], P. J. Wass[1], J. W. Conklin[1*]
[1] *University of Florida, Gainesville, Florida, 32611, USA and*
[2] *Imperial College London, Prince Consort Road, London. SW7 2AZ, UK*
(Dated: September 20, 2022)

We present a new technique for measuring the stray electric field in precision space inertial sensors by modulating the electric charge of a free-falling test mass and measuring the resulting coherent Coulomb force. The free charge of the test mass is controlled by ultraviolet photoemission using a pulsed light source synchronized with an oscillating potential capacitively induced on the test mass. We can modulate the test mass charge sinusoidally at an arbitrarily chosen frequency by varying the phase of the UV light pulses relative to the induced test mass potential at the appropriate rate. This technique allows us to optimize the precision of the measurement by choosing a modulation frequency that is within the most sensitive band of the sensor. We present an experimental validation of this approach using an inertial sensor integrated with a torsion pendulum, measuring the equivalent stray potential of the sensor with milliVolt precision in 10^4 s. We discuss the applicability of this technique for the upcoming Laser Interferometer Space Antenna (LISA) space gravitational-wave observatory and predict that the stray potential in LISA could be measured with < 0.1 mV precision in 200 s, assuming that a modulation frequency can be chosen that avoids gravitational wave signals.

I. INTRODUCTION

Precision space inertial sensors are an integral part of gravitational wave observatories [1–4], satellite geodesy missions [5, 6], and several fundamental physics experiments [7, 8]. These sensors are generally composed of a test mass (TM) in near free-fall, enclosed in an electrode housing (EH) that contains an array of electrodes that enable capacitive sensing and electrostatic actuation of the TM relative to the EH. An important source of force noise that can perturb the test mass from the desired pure free-fall is caused by stray electric fields that couple with test mass electric charge [9, 10]. The TM and EH surfaces exhibit "patch effects", a spatial variation in the electrostatic potential over nominally conducting surfaces [11] produced by surface contamination and areas of the metal surface in which different crystal orientations are exposed [12]. These patch effects combined with voltage offsets in the electronics connected to the sensor electrodes create a stray electric field across the EH that produces a Coulomb force on a charged TM.

Following the convention of [9], the stray field in the sensor can be modeled by an equivalent electrical potential Δ on a single electrode, that would create the same force or torque on the test mass. Considering the force F_x acting along the sensitive x axis of the instrument, in a symmetric sensor with a centered test mass and in the absence of other applied voltages,

$$F_x \approx -\frac{q}{C_T}\left|\frac{\partial C_x}{\partial x}\right|\Delta_x. \tag{1}$$

Here, C_T and C_x are the total capacitance of the TM to ground and the capacitance between the TM and the x-electrode. We commonly refer to the test mass potential relative to ground and due to charge as $V_{\rm TM} = \frac{q}{C_T}$. Force noise arises from either a fluctuating TM charge coupling with the mean value of Δ_x or a fluctuating Δ_x coupling with the mean test mass charge. Suppression of the former noise contribution, which is the focus of this work, is achieved by compensating for the mean Δ_x using applied dc voltages on the x-electrodes. The latter contribution is controlled by maintaining the TM charge near zero without aggravating the former using a charge management system (CMS).

A test mass CMS may employ a small, $\sim$10 μm diameter grounding wire, for example as in [5, 6, 8]. However, less noisy sensors use a non-contact UV photoemission-based technique. Previous missions have used Hg vapor lamps [13, 14], illuminating the TM or EH surface to discharge the test mass. However, for the upcoming LISA space gravitational wave mission [1, 2], ultraviolet (UV) light-emitting diodes (LED) will be used as the UV source [15, 16], primarily because of their improved lifetime, size, mass and power consumption compared with Hg lamps. Additionally, the high bandwidth (MHz) of LEDs enables pulsed operation, synchronized with oscillating electric fields between TM and EH [16, 17]. Driving the UV LEDs with pulse-width modulated current allows for a high dynamic range of generated UV power, while synchronization promotes electron transport in the desired direction. For the LISA inertial sensor, UV light pulses will be synchronized with a 100 kHz sinusoidal electric field used for capacitive sensing of TM position [18].

To compensate for the mean stray electric potential across the inertial sensor, Δ_x must be measured through a calibration procedure applying Eq. (1) to a measured F_x in response to a stimulus in q. One technique applies time-varying electrode voltages to capacitively induce a

* pwass@ufl.edu

coherent test mass potential equivalent to charge. However, the applied electrode voltages, coupling with patch potentials on the test mass produce a shear force on the TM, biasing the Δ_x measurement [19]. A more accurate approach uses UV light produced by the CMS to alter the charge on the test mass directly. This technique has been demonstrated using torsion pendula in the laboratory [19] and in space during the LISA Pathfinder mission [20], illuminating the TM or EH with UV light to achieve a step change in the charge and measuring the associated change in the dc force on the TM. While producing accurate results, the measurement technique is time-consuming, being limited by the performance of the instrument at low frequency and the time required to change the charge by UV illumination including settling time between steps. Typically in LISA Pathfinder a single measurement achieved a precision of around 1 mV for Δ_x for a measurement duration of 10,000 s. For LISA, Δ_x must be measured with similar precision to suppress the associated TM force noise to the point where it becomes sub-dominant in the overall sensitivity budget of the instrument. In this letter we present a technique with an experimental demonstration that allows for a periodic modulation of the free charge of the test mass using UV illumination at an arbitrarily chosen frequency. The technique allows the sensitivity of the measurement of Δ_x to be maximized and the possibility to combine multiple measurements separated in frequency within a system such as LISA with multiple TMs.

II. STRAY POTENTIAL MEASUREMENT USING CHARGE MODULATION

The test mass discharging properties can be understood by considering the test mass and electrode housing as two locally parallel surfaces. Electrons are emitted from one surface with some energy distribution and subject to a retarding or accelerating potential difference between the surfaces. In the absence of voltages applied to the electrodes in the EH, the relevant potential is that of the test mass ($V_{\rm TM} = q/C_T$). Electrons emitted with sufficient energy are able to traverse the gap between the TM and EH and contribute to a change in the test mass charge. The nature of the UV light injection and the reflectivity of the surfaces means that illumination of both surfaces simultaneously must be considered and the net discharging rate is the combination of contributions from the illumination of each surface.

The net discharge rate is characterized by the apparent yield (AY), defined in terms of the ratio of the observable macroscopic quantities: the TM charge rate and the UV power injected into the electrode housing. Analogous to the quantum yield of a surface, the apparent yield is expressed in units of electron charges per second $\dot{q}_e$, and the UV power in photons per second P_γ.

The dependence of AY on $V_{\rm TM}$ is characterized by positive and negative saturation values at which one of the discharging currents from the TM or EH is completely suppressed and the other is not suppressed at all and a transition region in which current flows from both surfaces in opposite directions. In this transition region there must exist a value for $V_{\rm TM}$ at which AY=0 and the test mass potential is stable and at equilibrium.

The measured AY for two different injection ports in our experimental setup described in the next section are shown in Fig. 1. While both curves show the expected sign dependence, the precise shape of the curve is a result of the UV illumination geometry, wavelength, surface quantum yields and work functions [21, 22], photoelectron energy distributions, and applied voltages on the inertial sensor electrodes [14, 23].

In our system, the energy of the illuminating UV photons (5.0 eV for $\lambda = 250$ nm) is near the work function of gold (4.4 eV for surfaces that have been exposed to air). In this regime, the dependence of photocurrent on $V_{\rm TM}$ from a single sensor surface is expected to be quadratic [22]. The combination of opposing currents produces a quasi-linear regime between the saturation values as AY passes through equilibrium. In the region of interest for test mass charge control, $|V_{\rm TM}| < 100$ mV, AY can be described as a linear function of $V_{\rm TM}$ with a slope β: AY $\propto -\beta V_{\rm TM}$. The region around AY=0 is highlighted in the inset to Fig. 1 showing a linear fit to the data.

Noting that AY $= \dot{q}_e/P_\gamma$, $\mathrm{d}V_{\rm TM}/\mathrm{d}t = \dot{q}_e C_T/e$ and the UV power, measured in Watts, $P_{\rm UV} = P_\gamma \lambda/hc$ where e is the elementary charge, $\lambda = 250$ nm is the wavelength of the UV light, h is Planck's constant, and c is the speed of light. Then we can write a differential equation $V_{\rm TM}$

$$\frac{\mathrm{d}V_{\rm TM}}{\mathrm{d}t} = -\frac{\beta e \lambda}{C_T hc P_{\rm UV}} V_{\rm TM}. \tag{2}$$

Considering the time-dependent behavior of the test mass potential under illumination near equilibrium and setting $\alpha = -\beta e\lambda/C_T hc$ we therefore have

$$V_{\rm TM}(t) = (V_0 - V_{\rm eq}) \exp(-\alpha t), \tag{3}$$

where V_0 and $V_{\rm eq}$ are the initial and equilibrium values of $V_{\rm TM}$ respectively. Physically, α is the decay constant of the test mass potential per unit power as the test mass tends to equilibrium under UV illumination.

In the behavior described above we have considered a continuous illumination scheme and the slowly varying component of the test mass potential, ignoring the charge exchange on the timescale of the 100 kHz oscillation of the test mass potential since it is typically not relevant for the test mass dynamics in the measurement bandwidth. The method of charge modulation that is the subject of this letter however, relies on a pulsed UV illumination phased-locked to an oscillating $V_{\rm TM}$. The test mass potential, considering also this time varying part, can be written $V_{\rm TM} = V_{\rm TM,DC} + V_{\rm inj} \sin 2\pi f t$ where $V_{\rm inj}$ is the amplitude of the capacitively-induced TM voltage bias at $f = 100$ kHz used for position sensing and $V_{\rm TM,DC}$ is the dc component of the test mass potential contributed by its free charge. The UV illumination

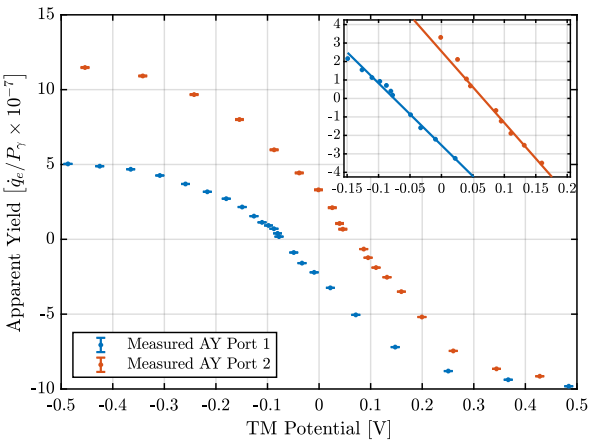


FIG. 1. Apparent yield (defined as test mass discharge rate per unit injected UV power) as a function of TM Potnetial for two UV injection ports in our inertial sensor shown in Figure 3. The inset shows the region close to AY= 0 in which we approximate the apparent yield as a linear function of TM potential. A linear fit to the data in this region is shown for each injection port.

phase with respect to the 100 kHz test mass potential is defined as $\phi = 2\pi f t_{\rm illum}$ with the time of illumination, $0 < t_{\rm illum} < 10\,\mu$s.

Setting a non-zero phase ϕ is equivalent to introducing an instantaneous shift in $V_{\rm TM}$ of $V_{\rm inj}\sin\phi$ seen by the pulsed photocurrents. The test mass accumulates charge, increasing $V_{\rm TM,DC}$ to compensate the shift, until it returns to its equilibrium value *at the periodic instants of illumination*. By this method we are able to set the test mass potential relevant to inertial sensor performance, $V_{\rm TM,DC}$, to any value $(V_{\rm eq} - V_{\rm inj}) < V_{\rm TM} < (V_{\rm eq} + V_{\rm inj})$ by shifting the illumination phase only. It follows that we can also drive an oscillation in the test mass potential by linearly varying the UV pulse phase $\phi(t) = 2\,\pi\,f_{\rm mod}\,t$. Since the test mass charge dynamics are governed by Eq.2, the resulting amplitude of the test mass modulation $V_{\rm TM,MOD}$ is filtered by the exponential decay constant α: $V_{\rm TM,MOD} = V_{\rm inj}/|(1 + i2\pi f_{\rm mod}/\alpha)|$.

III. EXPERIMENTAL DEMONSTRATION WITH A TORSION PENDULUM

We have experimentally demonstrated the charge modulation technique described in the previous section and used it to evaluate the stray electric field in an inertial sensor representative of that to be used in LISA [24] integrated into a torsion pendulum apparatus. The torsion pendulum at University of Florida has been designed as a test bed for LISA charge management technology development [25]. It consists of a suspended aluminum cross bar assembly with four hollow, precision-polished and gold-coated, test masses attached 0.22 m from its center. The cross bar is suspended from a 50 μm diameter, 1 m long, tungsten fiber. The low thermal noise of the suspension fiber along with the light-weighted test masses make the pendulum sensitive to forces acting on the test masses which are converted to pendulum torque by the arm of the cross bar. Two of the four TMs are housed in capacitive inertial sensors, one of which, shown diagramatically in Fig. 3 is representative of the LISA inertial sensor and is used for the charge modulation study described below. The entire pendulum assembly is housed in a vacuum chamber kept at a pressure of approximately 6×10^{-4} Pa. The vacuum chamber is housed in a thermally insulated room to provide passive temperature stabilization.

The orientation of the pendulum can be measured using a combination of the capacitive sensors on two opposing test masses and using a laser interferometer which measures the differential motion of the other two masses. The optical system typically has a lower readout noise and therefore is used in the analysis of the charge modulation experiments.

The electrostatic forces on the test mass by electric fields in the EH are derived from the torque acting on the pendulum. This in turn is derived from the angular readout, the known geometry and dynamics of the pendulum. The typical resulting force sensitivity is around 1 pN/Hz$^{1/2}$ at 1 mHz, limited by direct forces on the test mass and angular readout performance. Fig. 2 shows an example of the amplitude spectral density of the pendulum sensitivity to TM force noise representative of the performance achieved during the measurements reported here.

The test mass charge can be measured taking advantage of Eq. 1. Applying a voltage $V_{\rm meas}$ to the four electrodes on the x axis of the sensor, positive on the $+x$ and negative on $-x$ results in $\Delta_x = 4V_{\rm meas}$. Modulating $V_{\rm meas}$ produces a coherent force $F_{\rm meas}$ on the pendulum allowing the charge to be calculated $q = C_T F_{\rm meas}/4V_{\rm meas}|\frac{dC}{dx}|$. It is possible to apply the charge measurement modulation at a frequency well separated from the charge modulation frequency allowing for a continuous monitor of the test mass charge throughout all experiments.

The inertial sensor used for our charge modulation experiments is shown in Fig. 3. It has 12 electrodes used for capacitive sensing and electrostatic actuation on six degrees of freedom and six injection electrodes which provide the capacitively-induced test mass sensing bias. All injection electrodes are driven with a 4.4 V, 100 kHz sinusoidal signal resulting in an in-phase test mass potential modulation with an amplitude of $V_{\rm inj} = 406 \pm 10$ mV. The x-axis sensing and actuation electrodes are used for applying mHz charge measurement voltages and dc voltages to compensate Δ_x

UV light for photoelectric discharge is produced by a prototype version of the LISA charge management system electronics [26], which generates light pulses synchronized with the inertial sensor 100 kHz sensing bias. This

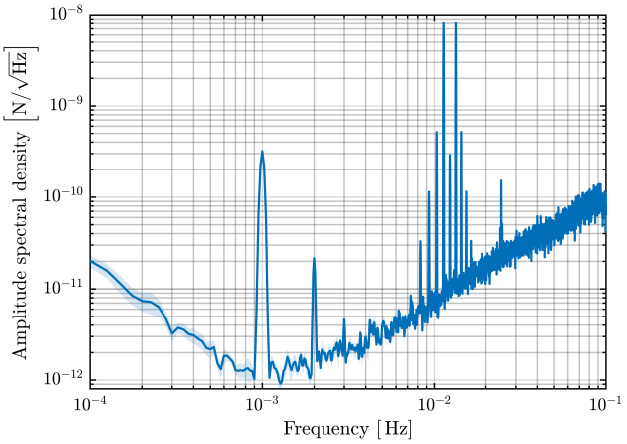


FIG. 2. Amplitude spectral density (ASD) of the force on the test mass in our torsion pendulum, F_x measured in the presence of a TM charge modulation at 1 mHz and a TM charge measurement at 12.3 mHz. The measurement shown represents 22680 s of data and the ASD has been calculated windowing the signal with 10, 40,000-s long Blackmann Harris windows with 50% overlap. The three lowest frequency points in the ASD which are polluted by spectral leakage from dc have been discarded. Note that charge modulation produces sidebands on the charge measurement signal.

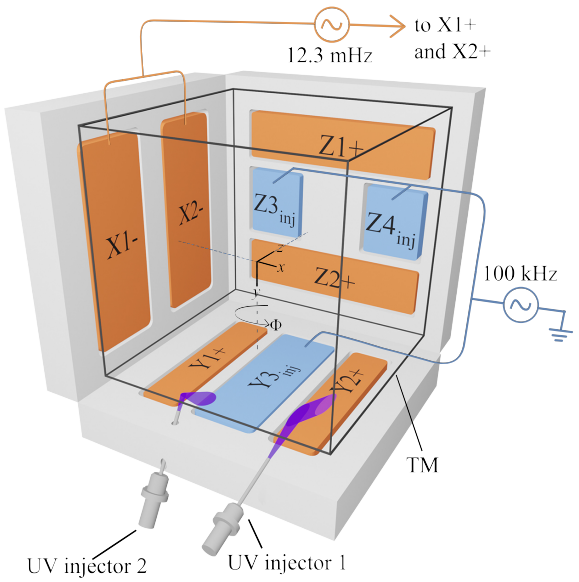


FIG. 3. Geometry of the test mass sensing/actuation electrodes (orange), injection electrodes (blue), and UV light injection (purple). The injected UV light in port 1 reflects off the TM and onto the Y2+ sensing/actuation electrode, whereas the light from port 2 reflects off the TM and onto the $Y3_{inj}$ electrode. Additional electrodes on opposing interior faces of the EH are not shown.

instrument allows commanding of the time-averaged UV power and phase of the pulsing with respect to the reference voltage from an experiment control computer. UV light is delivered to the electrode housing by multimode UV fiber optics through feedthroughs mounted on the vacuum chamber and fiber injectors inserted into the electrode housing.

Two UV injectors are used for this experiment, each illuminating EH surfaces in a different way and therefore with differing AY properties as shown in Fig. 1. UV injector 1 is directed toward the TM with a 75° angle of incidence relative to the surface normal and is centered on one of the sensing electrodes. In this geometry, most of the light is absorbed on the TM surface and the electrode opposite labelled Y2+ in Fig. 3. No voltages are applied to this electrode in our measurements. UV injector 2 is directed toward the TM with a 30° angle of incidence, between electrodes Y1+ and $Y3_{inj}$. The former has no applied voltages while the latter carries the 4.4 V 100 kHz capacitive sensing injection signal producing the V_{inj} modulation at 100 kHz on the test mass.

Illuminating the sensor with injector 1, and applying a phase modulation of the pulsed UV light creates a modulation about the TM equilibrium potential V_{eq} as described in Section II. A second pulsed UV illumination through injector 2, with a constant phase, was added to compensate for the non-zero V_{eq} and eliminate forces resulting from the coupling of the average test mass potential with its modulating component.

UV light was injected through injectors 1 and 2, phase-locked to the 100 kHz injection voltage with a 20% duty-cycle. The phase of the pulsed light from injector 1 was commanded digitally with a 1 mHz linear phase sweep as shown in the lower panel of Fig. 4. The time-averaged UV power from injector 1 was 207 nW and 178 nW through injector 2, including losses in the fiber chains. The TM potential was measured continuously by applying V_{meas} with an amplitude of 1 V at 12.3 mHz to the x-electrodes. The upper panel of Fig. 4 shows a short time span of charge measurement data, exhibiting the 1 mHz sinusoidal modulation.

The amplitude of the oscillating force and test mass charge were found by demodulating each at 1 mHz. Δ_x was calculated cycle-by-cycle using Eq. (1) and the measured values of F_x and V_{TM}, integrating over a measurement period of 10,000 s (10 cycles).

This measurement of was repeated while applying a range of dc compensation potentials V_{COMP} to the x-electrodes. Applying $+V_{COMP}$ to each of the $+x$ electrodes and $-V_{COMP}$ on $-x$, the resulting force becomes

$$F_x \approx -\frac{q}{C_T}\left|\frac{\partial C_x}{\partial x}\right|(\Delta_x + 4V_{COMP})\,. \qquad (4)$$

Measurements were made with applied V_{COMP} of -244 mV, -163 mV, -81 mV and $+81$ mV, The five measurements are shown in Fig. 5 and exhibit the linear dependence on the applied dc bias as expected from Eq. (4). The zero-compensation intercept gives the estimate for

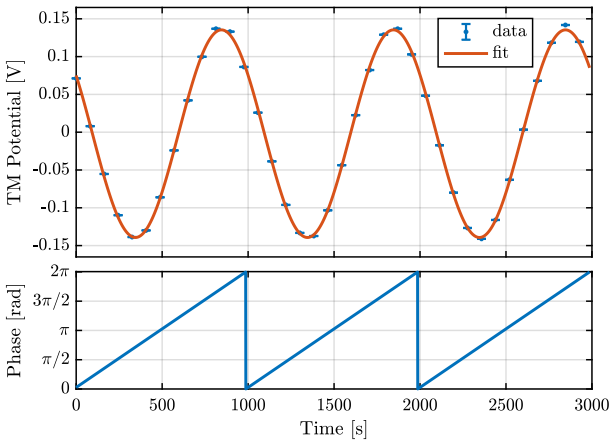


FIG. 4. Commanded phase of the UV pulses relative to the 100 kHz injection cycle (bottom) and the resulting sinusoidal variation in the measured TM potential (top).

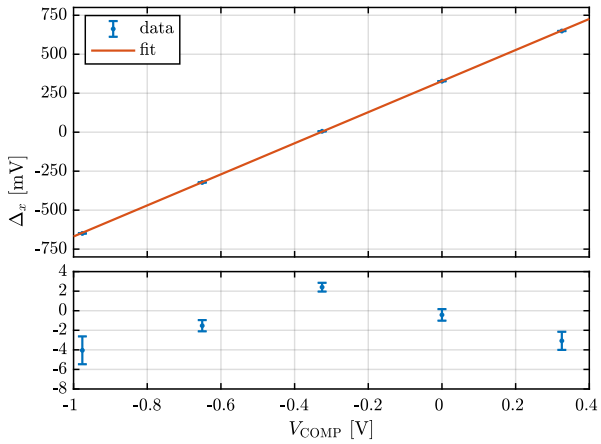


FIG. 5. The effective field in our inertial sensor along x, Δ_x as a function of the applied compensation voltages on the x electrodes V_{COMP}. Δ_x is calculated from the force acting on the TM at the charge modulation frequency and the amplitude of the charge modulation according to Eq. 1. Data with best-fit line (top) and fit residuals (bottom).

the inherent stray potential Δ_x. The value calculated from the best fit line is $-328.3 \pm 0.3\,\mathrm{mV}$ where the error quoted is the statistical error based on a weighted linear fit to the data. The slope of the line is 0.998 ± 0.001 in good agreement with the expected value of 1. The single point estimate for $\Delta_x = 327.4 \pm 0.3\,\mathrm{mV}$, derived from the force measured with no applied compensation also agrees well with the fit. However, the goodness of the fit ($\chi^2 = 25$) and scatter of the residuals indicate the presence of systematic errors not taken into account in the simplifying assumptions of Eq. (1).

The amplitude of the test mass potential modulation across all five measurements was 133-136 mV, measured with a precision of around 0.1 mV. The precision of the force measurement was around 20 fN while the amplitude of the observed electrostatic force was up to 25 pN. These measurement errors are in agreement with expected levels for a measurement limited by the torsion pendulum facility noise shown in Fig. 2. The force-noise performance of our pendulum facility also limits sensitivity to fluctuations in Δ_x to the level of $20\,\mathrm{mV/Hz^{1/2}}$, well above the level of variation observed in similar sensors [19, 20, 27].

IV. DISCUSSION AND CONCLUSIONS

We have demonstrated a novel technique to measure the coupling between stray electric fields and test mass charge in an electrostatic test mass position sensor. The measurement uncertainty is consistent with facility noise. The expected force noise floor of a single LISA sensor of $6\,\mathrm{fN/Hz^{1/2}}$ has been demonstrated in space [28]. In applying the technique to a gravitational wave observatory such as LISA, other constraints should be considered. Firstly, that the maximum sensitivity requires a measurement distributed between multiple spacecraft and secondly, that gravitational wave signals will be present in the sensitive axis.

A measurement of the TM potential modulation can be made by exciting forces or torques in non-sensitive degrees of freedom of the instrument, which can be measured locally on one LISA spacecraft with good precision. The resulting force coupling with stray fields however, is only relevant to the instrument performance measured along the sensitive axes of the LISA constellation, between test masses in distant spacecraft. To overcome laser frequency noise in the position measurement between test masses, a differential measurement in two LISA arms is required using the time-delay interferometry method [29, 30].

As an illustrative example, we choose a charge modulation frequency of 5 mHz. The LISA force sensitivity at this frequency would be $24\,\mathrm{fN/Hz^{1/2}}$ assuming the inertial sensor performance above and an interferometer optical readout noise of $10\,\mathrm{pm/Hz^{1/2}}$. At 5 mHz with $V_{\mathrm{inj}} = 0.6\,\mathrm{V}$ for the LISA sensor using an apparent yield as measured in our sensor, the amplitude of the test mass charge modulation would be around 110 mV. With $\left|\frac{\partial C_x}{\partial x}\right| = 292\,\mathrm{pF/m}$ for the LISA inertial sensor and considering instrument noise alone, Δ_x can be measured with a precision of $53\,\mu\mathrm{V}$ in one 200 s cycle, which is roughly 20 times better than the mV-level required, indicating that lower UV powers and lower charge modulation amplitudes could be used.

It is expected that the amplitude of continuous gravitational wave (GW) signals will be significantly higher than the instrument noise level. However, the ability to choose an arbitrary measurement frequency for the calibration, and the fact that the expected signal is relatively high means that the calibration should be effective even in the presence of a strong GW background.

Significant uncertainty remains in the shape of the apparent yield curve for LISA-like sensors, and therefore the resulting corner frequency for charge modulation, α, which depends on the quantum yield and work functions of the surfaces. Although the AY slope at equilibrium is not directly comparable with the results presented in [14], which used a continuous illumination, the apparent yields at the extremes of the AY curve are comparable and are somewhat higher than those found in this work. With all other parameters equal, higher yields result in higher cut-off frequencies and larger charge modulation and improved sensitivity. Based on the expected variability of gold surface quantum yields, it is not expected that the slope of the AY curve in LISA would be less than half of the value measured value here. This would reduce the amplitude of the charge modulation (by a factor up to 1/2) but the calibration signal sensitivity would remain very high.

The charge modulation technique described in this letter therefore would allow the stray potential in the LISA inertial sensor to be determined with sufficient precision to compensate it and suppress random test mass charging noise in a measurement period of 200 s or less, even in the presence of large gravitational wave signals. In principle, the measurement can be made simultaneously on multiple test masses by separating the modulations in frequency. Comparing with the technique demonstrated during the LISA Pathfinder mission, which determined Δ_x from the DC force change produced by a step change in test mass charge, time-savings are significant.

ACKNOWLEDGMENTS

The authors would like to thank William Weber and Rita Dolesi from the University of Trento for helpful discussions and insights into prior stray potential measurement techniques. This research was made possible by NASA LISA Charge Management System grant 80NSSC17K0277 and NASA N.G. Roman Technology Fellowship grant NNX15AF26G. TJS acknowledges support from the Leverhulme Trust (EM-2019-070\4).

[1] eLISA Consortium and Others, "The Gravitational Universe," *arXiv e-prints*, p. arXiv:1305.5720, may 2013.

[2] P. Amaro-Seoane *et al.*, "Laser Interferometer Space Antenna," *arXiv e-prints*, p. arXiv:1702.00786, Feb. 2017.

[3] J. Luo *et al.*, "TianQin: a space-borne gravitational wave detector," *Classical and Quantum Gravity*, vol. 33, no. 3, p. 035010, Feb. 2016.

[4] G. Jin, "Program in space detection of gravitational wave in Chinese Academy of Sciences," in *Journal of Physics Conference Series*, ser. Journal of Physics Conference Series, vol. 840, May 2017, p. 012009.

[5] P. Touboul, B. Foulon, B. Christophe, and J. P. Marque, "CHAMP, GRACE, GOCE Instruments and Beyond," in *Geodesy for Planet Earth*. Springer, 2012, pp. 215–221. [Online]. Available: https://link.springer.com/chapter/10.1007/978-3-642-20338-1{_}26

[6] B. Christophe *et al.*, "A new generation of ultra-sensitive electrostatic accelerometers for GRACE Follow-on and towards the next generation gravity missions," *Acta Astronautica*, vol. 117, no. September 2010, pp. 1–7, 2015. [Online]. Available: http://dx.doi.org/10.1016/j.actaastro.2015.06.021

[7] C. W. F. Everitt *et al.*, "The Gravity Probe B test of general relativity," *Classical and Quantum Gravity*, vol. 32, no. 22, p. 224001, 2015. [Online]. Available: https://iopscience.iop.org/article/10.1088/0264-9381/32/22/224001

[8] P. Touboul *et al.*, "Microscope mission: First results of a space test of the equivalence principle," *Phys. Rev. Lett.*, vol. 119, p. 231101, Dec 2017. [Online]. Available: https://link.aps.org/doi/10.1103/PhysRevLett.119.231101

[9] W. J. Weber *et al.*, "Possibilities for measurement and compensation of stray DC electric fields acting on drag-free test masses," *Advances in Space Research*, vol. 39, no. 2, pp. 213–218, 2007.

[10] T. J. Sumner, G. Mueller, J. W. Conklin, P. J. Wass, and D. Hollington, "Charge induced acceleration noise in the LISA gravitational reference sensor," *Classical and Quantum Gravity*, vol. 37, no. 4, p. 045010, 2020. [Online]. Available: https://doi.org/10.1088/1361-6382/ab5f6e

[11] C. C. Speake and C. Trenkel, "Forces between conducting surfaces due to spatial variations of surface potential," *Phys. Rev. Lett.*, vol. 90, p. 160403, Apr 2003. [Online]. Available: https://link.aps.org/doi/10.1103/PhysRevLett.90.160403

[12] J. B. Camp, T. W. Darling, and R. E. Brown, "Effect of crystallites on surface potential variations of Au and graphite," *Journal of Applied Physics*, vol. 71, no. 2, pp. 783–785, 1992.

[13] S. Buchman, T. Quinn, G. M. Keiser, D. Gill, and T. J. Sumner, "Charge measurement and control for the Gravity Probe B gyroscopes," *Review of Scientific Instruments*, vol. 66, no. 1, pp. 120–129, 1995.

[14] M. Armano *et al.*, "Precision charge control for isolated free-falling test masses: Lisa pathfinder results," *Phys. Rev. D*, vol. 98, p. 062001, Sep 2018. [Online]. Available: https://link.aps.org/doi/10.1103/PhysRevD.98.062001

[15] D. Hollington, J. T. Baird, T. J. Sumner, and P. J. Wass, "Characterising and testing deep UV LEDs for use in space applications," *Classical and Quantum Gravity*, vol. 32, no. 23, 2015.

[16] T. Olatunde *et al.*, "240 nm UV LEDs for LISA test mass charge control," *Journal of Physics: Conference Series*, vol. 610, no. 1, 2015.

[17] K. X. Sun, B. Allard, S. Buchman, S. Williams, and R. L. Byer, "LED deep UV source for charge management of gravitational reference sensors," *Classical and Quantum Gravity*, vol. 23, no. 8, 2006.

[18] T. Ziegler, P. Bergner, G. Hechenblaikner, N. Brandt,

and W. Fichter, "Modeling and performance of contact-free discharge systems for space inertial sensors," *IEEE Transactions on Aerospace and Electronic Systems*, vol. 50, no. 2, pp. 1493–1510, 2014.

[19] F. Antonucci *et al.*, "Interaction between stray electrostatic fields and a charged free-falling test mass," *Phys. Rev. Lett.*, vol. 108, p. 181101, Apr 2012. [Online]. Available: https://link.aps.org/doi/10.1103/PhysRevLett.108.181101

[20] M. Armano *et al.*, "Charge-induced force noise on free-falling test masses: Results from lisa pathfinder," *Phys. Rev. Lett.*, vol. 118, p. 171101, Apr 2017. [Online]. Available: https://link.aps.org/doi/10.1103/PhysRevLett.118.171101

[21] T. Olatunde *et al.*, "Characterisation of Au surface properties relevant for UV photoemission- based charge control for space inertial sensors Characterisation of Au surface properties relevant for UV photoemission-based," *Classical and Quantum Gravity*, 2020.

[22] P. J. Wass, D. Hollington, T. J. Sumner, F. Yang, and M. Pfeil, "Effective decrease of photoelectric emission threshold from gold plated surfaces," *Review of Scientific Instruments*, vol. 90, no. 6, 2019. [Online]. Available: http://dx.doi.org/10.1063/1.5088135

[23] H. Inchauspé *et al.*, "Numerical modeling and experimental demonstration of pulsed charge control for the space inertial sensor used in lisa," *Phys. Rev. D*, vol. 102, p. 042002, Aug 2020. [Online]. Available: https://link.aps.org/doi/10.1103/PhysRevD.102.042002

[24] R. Dolesi *et al.*, "Gravitational sensor for LISA and its technology demonstration mission," *Classical and Quantum Gravity*, vol. 20, no. 10, 2003.

[25] G. Ciani *et al.*, "A new torsion pendulum for gravitational reference sensor technology development," *Review of Scientific Instruments*, vol. 88, no. 6, p. 64502, 2017.

[26] S. Parry Kenyon *et al.*, "A Charge Management System for Gravitational Reference Sensors – Design and Instrument Testing," *IEEE Aerospace Conference Proceeding*, 2021.

[27] S. E. Pollack, S. Schlamminger, and J. H. Gundlach, "Temporal extent of surface potentials between closely spaced metals," *Phys. Rev. Lett.*, vol. 101, p. 071101, Aug 2008. [Online]. Available: https://link.aps.org/doi/10.1103/PhysRevLett.101.071101

[28] M. Armano *et al.*, "Beyond the required lisa free-fall performance: New lisa pathfinder results down to 20 μHz," *Phys. Rev. Lett.*, vol. 120, p. 061101, Feb 2018. [Online]. Available: https://link.aps.org/doi/10.1103/PhysRevLett.120.061101

[29] J. W. Armstrong, F. B. Estabrook, and M. Tinto, "Time-Delay Interferometry for Space-based Gravitational Wave Searches," *Astrophys. J.*, vol. 527, no. 2, pp. 814–826, Dec. 1999.

[30] M. Tinto and S. V. Dhurandhar, "Time-delay interferometry," *Living reviews in relativity*, vol. 17, no. 1, p. 6, 2014. [Online]. Available: https://europepmc.org/articles/PMC5253929